Bioinorganic Chemistry

Proton Switch in the Secondary Coordination Sphere to Control Catalytic Events at the Metal Center: Biomimetic Oxo Transfer Chemistry of Nickel Amidate Complex

Soohyung Kim,[a] Ha Young Jeong,[b] Seonghan Kim,[c] Hongsik Kim,[a] Sojeong Lee,[b] Jaeheung Cho,*[c, d] Cheal Kim,*[b] and Dongwhan Lee*[a]

Abstract: High-valent metal-oxo species are key intermediates for the oxygen atom transfer step in the catalytic cycles of many metalloenzymes. While the redox-active metal centers of such enzymes are typically supported by anionic amino acid side chains or porphyrin rings, peptide backbones might function as strong electron-donating ligands to stabilize high oxidation states. To test the feasibility of this idea in synthetic settings, we have prepared a nickel(II) complex of new amido multidentate ligand. The mononuclear nickel complex of this N5 ligand catalyzes epoxidation reactions of a wide range of olefins by using mCPBA as a terminal oxidant. Notably, a remarkably high catalytic efficiency and selectivity were observed for terminal olefin substrates. We found that protonation of the secondary coordination sphere serves as the entry point to the catalytic cycle, in which high-valent nickel species is subsequently formed to carry out oxo-transfer reactions. A conceptually parallel process might allow metalloenzymes to control the catalytic cycle in the primary coordination sphere by using proton switch in the secondary coordination sphere.

Introduction

Nature has evolved efficient strategies to transfer oxygen atoms to hydrocarbons by using iron,[1] copper,[2] or manganese[3] dependent metalloenzymes. In such biological catalysis, high-valent metal-oxo species are often involved as key intermediates.[4] To help access the high oxidation states of the metal, the active sites of metalloenzymes exploit anionic ligands derived from amino acid side chains or porphyrin derivatives.[5] A few rare examples of metalloenzymes, however, utilize peptide backbone itself to supply anionic ligand donors.[6]

Nitrile hydratases (NHases) hydrolyze nitriles into amides. The active site of cobalt-based NHase (Figure 1 a) is comprised of two monoanionic amidate nitrogen atoms from the peptide backbone and three sulfur atoms from amino acid side chains.[7] For a finer control over the Lewis acidity and redox properties of the metal center, hydrogen bonding networks cooperatively exert secondary coordination sphere effects.[8] As another example, nickel superoxide dismutase (NiSOD) catalyzes the disproportionation of superoxide to produce dioxygen and hydrogen peroxide.[9] The reaction mechanism requires cycling between nickel(II) and nickel(III) oxidation states, al-

[a] S. Kim, H. Kim, Prof. Dr. D. Lee
Department of Chemistry, Seoul National University
1 Gwanak-ro, Gwanak-gu, Seoul 08826 (Korea)
E-mail: dongwhan@snu.ac.kr
[b] H. Y. Jeong, S. Lee, Prof. Dr. C. Kim
Department of Fine Chemistry
Seoul National University of Science and Technology
232 Gongneung-ro, Nowon-gu, Seoul 01811 (Korea)
E-mail: chealkim@seoultech.ac.kr
[c] S. Kim, Prof. Dr. J. Cho
Department of Emerging Materials Science, DGIST
Daegu 42988 (Korea)
[d] Prof. Dr. J. Cho
Department of Chemistry
Ulsan National Institute of Science and Technology (UNIST)
Ulsan 44919 (Korea)
E-mail: jaeheung@unist.ac.kr
Supporting information and the ORCID identification numbers for the authors of this article can be found under: https://doi.org/10.1002/chem.202005183.

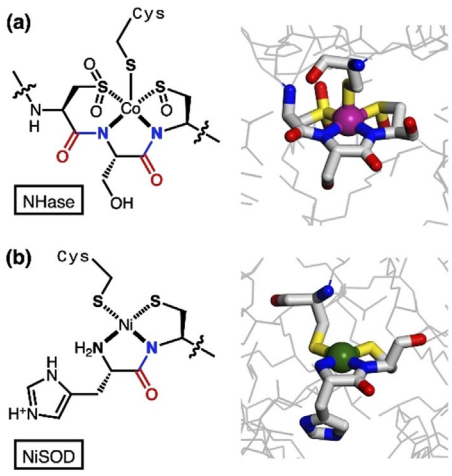

Figure 1. Chemical structures of the active sites of (a) cobalt-based NHase and (b) NiSOD. Shown next is the X-ray structure of each enzyme (PDB code: 1IRE for cobalt-based NHase; 1T6U for NiSOD).

though the redox chemistry of nickel in non-porphyrinoid setting is challenging under biological conditions.[10] In the active site of NiSOD, the metal center is coordinated to the ligands derived from cysteine thiolates, N-terminal amine, and deprotonated amide backbone (Figure 1 b). The peptidyl *N*-amidate ligand here helps stabilize the oxidized nickel(III) species and prevent the deleterious oxidation of cysteine sulfur atoms.[11]

As synthetic systems inspired by metalloenzymes, nickel-based catalysts can carry out hydroxylation of alkanes and epoxidation of alkenes using H_2O_2, mCPBA, or NaOCl as terminal oxidant.[12] To accommodate high-valent nickel-oxo species as active oxidants in the catalytic cycle, various nickel complexes have been developed that are supported by electron-rich ligands having anionic amidate or neutral guanidyl motif.[12f–k] Only a few nickel-based catalytic systems, however, are currently available for efficient epoxidation of terminal olefins with high selectivity under mild conditions.[13]

In this study, we report the chemistry of a new pentadentate ligand H-dpap (dpap = 2-(di(pyridin-2-ylmethyl)amino)-*N*-(2-(5-methylpyridin-2-yl)phenyl)acetamidate) and its mononuclear nickel complex [Ni^{II}(dpap)](ClO_4) (**1**), which functions as an efficient catalyst for the epoxidation of various terminal olefins. Due to their electron deficient nature, terminal olefins are a particularly challenging class of substrates to epoxidize. Since terminal epoxides are useful building blocks for the synthesis of value-added organic molecules, developing an efficient catalyst is a topic of both fundamental and practical importance.[14]

Results and Discussion

Ligand design and synthesis

The dpap ligand system is based on the N3 ligand **2** (Figure 2 a) which we recently reported for biomimetic iron chemistry.[15] The first-generation tridentate ligand **2** was prepared by installing a flexible pyridyl pendant to the rigid and π-conjugated anilido-pyridyl [*N*,*N*]-bidentate motif **3**. To stabilize the high-valent metal-oxo species, we have increased the ligand denticity by appending the tridentate bis(2-pyridylmethyl)amine tether to the bidentate **3** by using an amide linker (Figure 2 a).

Upon metallation, the amide N–H group of H-dpap is deprotonated to afford monoanionic ligand dpap. As shown in Figure 2 b, the amide carbonyl group of the dpap ligand is not directly coordinated to the metal, but protonation or metal-binding to this secondary coordination sphere can reversibly modulate the relative contribution of the amido vs. iminol/iminolate Lewis structure descriptions in resonance, thereby enabling remote control of the ligand donor ability.[16] The ligand H-dpap was conveniently prepared by an amide coupling reaction between **3**[15] and **4**[17] in excellent yield (> 95 %) (Scheme 1).

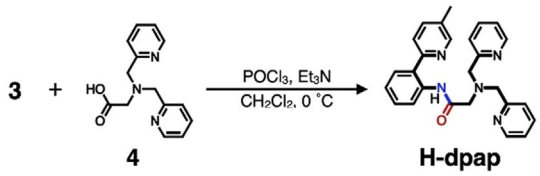

Scheme 1. Synthesis of H-dpap ligand.

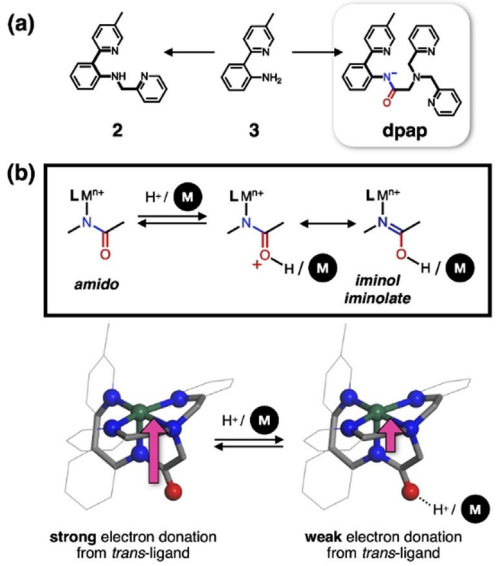

Figure 2. (a) Functionalization of anilido-pyridine to increase the denticity and electron-donating ability of the ligand. (b) Modulation of secondary coordination sphere by protonation or binding of Lewis acidic metal to the amide carbonyl group.

Preparation and characterization of nickel(II) complex

Mononuclear nickel complex **1** was synthesized from Ni(ClO_4)$_2$·6 H_2O and H-dpap in the presence of Et_3N in MeCN. The resulting light purple precipitate was isolated by filtration, and washed with MeCN and Et_2O. The crude product was purified by crystallization from MeOH/Et_2O, which also produced single-crystals suitable for X-ray crystallography (Figure 3 a).

As anticipated, the nickel center in the cation of **1** is coordinated to all of the five nitrogen atoms of the monoanionic ligand. Among the five Ni–N bonds, the axial Ni–N1 distance (2.016(2) Å) is the shortest, which reflects the strong electron donor ability of the anionic amidate-*N*. Intriguingly, the open axial site of the complex is taken up by the carbonyl oxygen atom of adjacent **1** unit to complete a *pseudo*-octahedral geometry (Figure 3 b). As shown in Figure 2 b, metal binding enhances the contribution of the iminolate over the amido character, thereby attenuating the electron-donating ability of the nitrogen atom of the amide group. Such a cascade transmission of electronic effect is best accommodated in a one-dimensional (1D) polymeric structure in the solid state.[18] When the 1D coordination polymer dissolves in polar solvent MeCN, however, the weak Ni–$O_{carbonyl}$ bond would dissociate so that a pentacoordinate nickel complex could be generated with a vacant axial site for substrate binding and subsequent reaction chemistry. We proceeded to test this idea with oxo group transfer reactions to olefinic substrates.

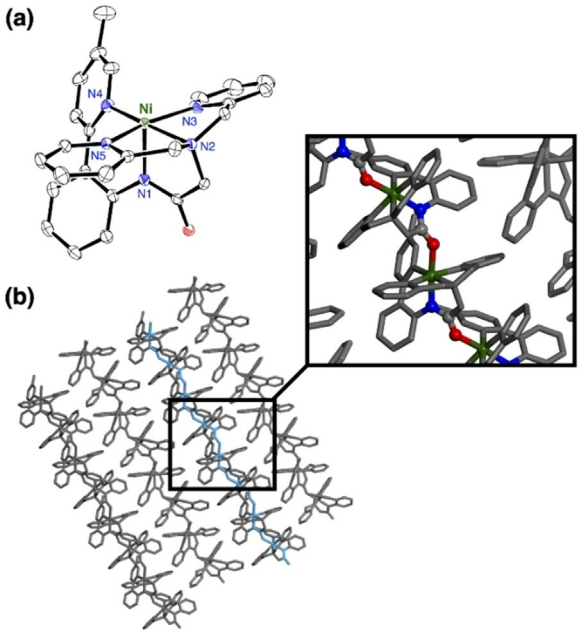

Figure 3. (a) ORTEP diagram of the cation of **1** with thermal ellipsoids at the 50% probability level. Hydrogen atoms are omitted for clarity. (b) Capped-stick representation of 1D polymeric packing of **1** and a close-up view. The ClO_4^- counter anions are omitted for clarity.

Table 1. Epoxidation of olefins catalyzed by **1**.[a]

Entry	Substrate	Product	Conversion (%)[b]	Yield (%)[b]
1	cyclopentene	epoxide	≈100	63.2±2.8
2	cycloheptene	epoxide	≈100	≈100
3	cyclooctene	epoxide	98.0±0.1	59.2±0.5
4	cyclohexene	epoxide	97.9±0	82.3±3.5
		2-cyclohexenol		trace
		2-cyclohexenone		4.3±0
5	1-hexene	epoxide	63.1±1.4	50.5±5.2
6	1-octene	epoxide	71.5±1.1	46.5±0.9
7	*cis*-2-hexene	*cis*-oxide	97.0±0.2	30.0±0.2
		trans-oxide		62.6±0.7
8	*trans*-2-hexene	*trans*-oxide	≈100	85.5±1.2
9	*cis*-2-octene	*cis*-oxide	≈100	32.1±3.0
		trans-oxide		61.0±6.9
10	*trans*-2-octene	*trans*-oxide	99.2±0.4	72.1±1.2
11	styrene	epoxide	≈100	62.7±1.8
		benzaldehyde		3.8±0.2
		phenylacetaldehyde		12.1±0.7
12	*cis*-stilbene	*cis*-stilbene oxide	≈100	9.3±0.1
		trans-stilbene oxide		63.4±4.8
		benzaldehyde		7.3±0.7
		2-phenylacetophenone		trace
13	*trans*-stilbene	*trans*-stilbene oxide	≈100	53.0±1.2
		benzaldehyde		7.5±0.1
		2-phenylacetophenone		trace

[a] Reaction conditions: substrates (0.035 mmol), **1** (0.0017 mmol), and mCPBA (0.10 mmol) in MeCN (1 mL), $T = 25\,^{\circ}C$. [b] Based on the substrate.

Olefin epoxidation reactions

Using **1** as an oxo-transfer catalyst and mCPBA as a terminal oxidant, olefin epoxidation reactions were carried out for a wide range of olefin substrates listed in Table 1. At r.t., the reactions were complete within <10 min in MeCN. In the absence of **1**, however, direct epoxidation of substrates by mCPBA alone was negligible (Table S2).

As reported in Table 1, cyclic olefins (entries 1–3) were converted to the corresponding epoxides in moderate to excellent yields (59.2–100%). Cyclohexene was oxidized to cyclohexene oxide (82.3%, entry 4) as the major product, along with small amounts of byproducts such as 2-cyclohexenone (4.3%) and 2-cyclohexenol (trace). Terminal olefins such as 1-hexene and 1-octene (entries 5 and 6) are challenging substrates to oxidize. We found that **1** epoxidized them in moderate yields (47–51%). Previously reported non-heme nickel complexes and porphyrin nickel complexes typically show low catalytic activity towards terminal olefins.[12c,j]

To study the stereochemistry of the epoxidation reaction, *cis*-2-hexene and *cis*-2-octene (entries 7 and 9) were used. They were mainly converted to *trans*-2-hexene oxide (62.6%) and *trans*-2-octene oxide (61.0%), along with lower amounts of *cis*-2-hexene oxide (30.0%) and *cis*-2-octene oxide (32.1%). When *trans*-2-hexene and *trans*-2-octene (entries 8 and 10) were used, *trans*-2-hexene oxide (85.5%) and *trans*-2-octene oxide (72.1%) were obtained. These results implicate that the putative Ni-oxo-olefin radical intermediate has sufficiently long lifetime, to allow for the rotation of the initially formed Ni-oxo-*cis*-olefin radical to the thermodynamically more stable *trans*-olefin radical (Scheme S1).[19]

Styrene was oxidized to styrene oxide (62.7%, entry 11) along with small amounts of benzaldehyde (3.8%) and phenylacetaldehyde (12.1%). For *cis*-stilbene (entry 12), *trans*-stilbene oxide (63.4%) was formed as the major product with a small amount of *cis*-stilbene oxide (9.3%); *trans*-stilbene (entry 13) was transformed to *trans*-stilbene oxide (53.0%) as the major product along with benzaldehyde byproduct (7.5%). The formation of aldehyde and ketone products from aromatic olefins suggests that certain amount of peroxyl radical species participates as active oxidants in the catalytic reactions.[12a,20]

Epoxidation of terminal olefins

The epoxidation of terminal olefins is an important class of functional group transformation. The resulting 1,2-epoxide products are versatile building blocks for the synthesis of useful organic molecules.[14] Since our nickel-based catalytic system showed promising reactivity towards terminal olefins (entries 5 and 6, Table 1), we proceeded to examine the epoxidation reactions of an expanded set of terminal olefins. Under standard conditions, various terminal olefins reacted in excellent conversion (93.6–100%) to afford the epoxidation products up to 90% yield (Table 2). The selectivity showed a gradual decrease with increasing chain length. No nickel-based catalysts are currently known that effect catalytic epoxidation of terminal olefins with such high efficiency and selectivity.[12c,j]

Table 2. Epoxidation of terminal olefins catalyzed by **1**.[a]

Entry	Substrate	Product	Conversion (%)[b]	Yield (%)[b]
1	1-hexene	1,2-epoxyhexane	≈100	89.5±0.7
2	1-octene	1,2-epoxyoctane	93.9±0.5	72.8±1.2
3	1-nonene	1,2-epoxynonane	96.4±0.5	69.4±2.1
4	1-decene	1,2-epoxydecane	96.9±0.4	52.8±2.0
5	1-undecene	1,2-epoxyundecane	95.9±0.6	44.0±1.2
6	1-dodecene	1,2-epoxydodecane	99.9±0.1	44.3±1.9
7	1-tridecene	1,2-epoxytridecane	98.0±0.2	35.4±3.8
8	1-tetradecene	1,2-epoxytetradecane	99.1±0.1	20.3±3.8
9	1-pentadecene	1,2-epoxypentadecane	96.5±0.1	31.6±0.8
10	1-hexadecene	1,2-epoxyhexadecane	≈100	37.8±3.8
11	1-octadecene	1,2-epoxyoctadecane	≈100	18.4±0.9
12	vinylcyclohexane	vinylcyclohexane oxide	93.6±2.1	60.0±1.7

[a] Reaction conditions: substrates (0.020 mmol), **1** (0.0017 mmol), and mCPBA (0.20 mmol) in MeCN (1 mL), $T = 25\,^{\circ}C$. [b] Based on the substrate.

Reversible protonation of nickel complex

To elucidate the mechanism of oxygen atom transfer reaction described above, we first performed a cold spray ionization mass spectrometry (CSI-MS) analysis of an MeCN solution sample of **1**. Only one prominent peak was observed at $m/z = 480.2$, which corresponds to the mass of discrete $[Ni^{II}(dpap)]^+$ species (calcd $m/z = 480.1$) (Figure 4a). The isotopic patterns for the observed ions further validated this assignment (Figure S1). Upon addition of mCPBA to the solution, new peaks at $m/z = 240.6$ and $m/z = 261.1$ appeared, which correspond to the $[Ni^{II}(dpap)(H)]^{2+}$ (calcd $m/z = 240.6$) and $[Ni^{II}(dpap)(MeCN)(H)]^{2+}$ (calcd $m/z = 261.1$) species, respectively. However, its conjugate base $[Ni^{II}(dpap)(MeCN)]^+$ (calcd $m/z = 521.2$) was not detected under the same condition (Figure 4b). To confirm that this shift in solution population is indeed triggered by protonation, 1 equiv of $HClO_4$ was added to the solution sample of **1**. The same peak at $m/z = 261.1$ for $[Ni^{II}(dpap)(MeCN)(H)]^{2+}$ was detected, but no peak was observed at $m/z = 521.2$ for $[Ni^{II}(dpap)(MeCN)]^+$ (Figure S2 and Figure S3).

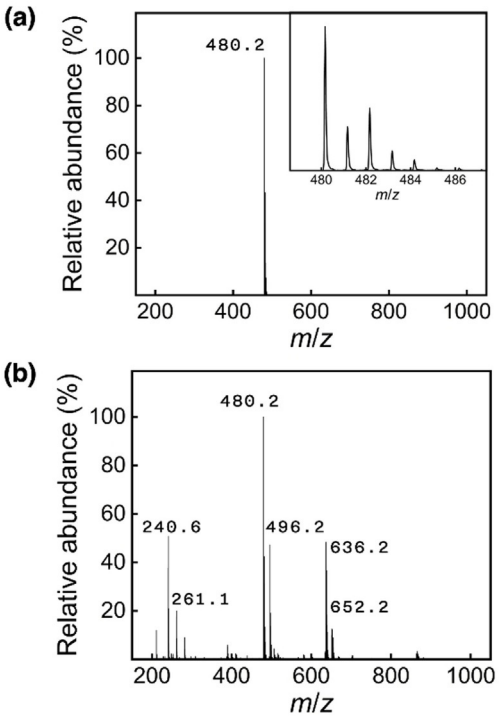

Figure 4. Positive-ion CSI-MS spectra ($T = 233$ K) of (a) **1** in MeCN (concentration = 0.1 mM), and (b) after treatment with mCPBA (2 equiv). Inset shows the observed isotope distribution pattern.

These results suggest that protonation lowers the electron donating ability of the ligand (Figure 2b), so that MeCN solvent molecule is recruited as the sixth ligand to balance the overall electronic demand of the metal center. It is reasonable to speculate that the position of protonation is the amide carbonyl oxygen atom when analogy is drawn to the X-ray structure shown in Figure 3b.[21] Here, Lewis acidic nickel(II) center of the adjacent repeat unit of the coordination polymer in the solid-state takes the role of proton in solution.

In support of this interpretation, the DFT computed (UBP86/Def2-TZVP level of theory) Mulliken charge of the carbonyl oxygen atom is −0.33, which is the most negative among all the heteroatoms within **1** (Table S3). The molecular electrostatic potential (MEP) map of **1** (Figure S4) also shows that the carbonyl oxygen atom is the most electron-rich site to be targeted by the proton. Indeed, the geometry optimized DFT models of protonated $[Ni^{II}(dpap)(H)]^{2+}$ (Figure S5) predict that the oxygen-protonated isomer should be the energetically most preferred form when the proton is allowed to choose any of the Brønsted basic N- or O-donor atoms of $[Ni^{II}(dpap)]^+$.

In our mass spectrometric analysis, a peak at $m/z = 652.2$ was also observed (Figure 4b), which corresponds to the $[Ni^{II}(dpap)(mCPBA)]^+$ (calcd $m/z = 652.1$) species. This finding implies that mCPBA used as a terminal oxidant can also coordinate to the vacant site of nickel center. A peak at $m/z = 496.2$ was also observed, which could be assigned to the $[Ni^{IV}(dpap)(O)]^+$ (calcd $m/z = 496.1$) species.

A coherent mechanistic picture emerges from the CSI-MS analysis of **1** in solution. As postulated in Scheme 2, protonation event in the ligand sphere controls the electronic demand of the metal sphere. When mCPBA is added to the solution for the epoxidation reaction, the released proton should first bind

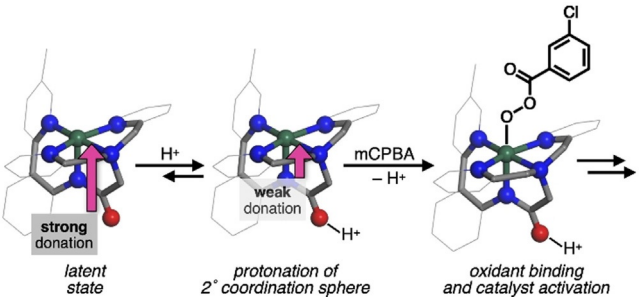

Scheme 2. Proposed mechanism of oxidant binding to the metal center triggered by protonation of the secondary coordination sphere.

to the amide carbonyl group. The attenuated electron-donating ability of the amide group of the ligand facilitates coordination of the peroxycarboxylate unit of mCPBA to the vacant site of $[Ni^{II}(dpap)(H)]^{2+}$. Both intermediates $[Ni^{II}(dpap)(H)]^{2+}$ and $[Ni^{II}(dpap)(mCPBA)]^{+}$ were observed by CSI-MS analysis (Figure 4b). The entry point into the catalytic cycle is thus gated by mCPBA functioning first as a Brønsted acid, and subsequently as metal-bound oxidant (Scheme 2).

To follow this intriguing solution chemistry, we carried out UV/Vis spectroscopic studies while adding $HClO_4$ to the metal complex and back-titrating with Et_3N. As a proton donor, perchloric acid was chosen to avoid complications from anion coordinating to the metal center. As shown in Figure 5a, the UV/Vis spectra of **1** in MeCN displayed an increase in the absorption at $\lambda_{max} = 250$ nm with concomitant decrease at $\lambda_{max} = 350$ nm upon addition of up to 1 equiv $HClO_4$. Subsequent addition of Et_3N (1 equiv) restored the original spectrum, thus establishing the reversible nature of the protonation-induced interconversion between $[Ni^{II}(dpap)]^{+}$ and $[Ni^{II}(dpap)(MeCN)(H)]^{2+}$ (Scheme 2). The presence of isosbestic points is consistent with the equilibrium between two spectroscopically observable species.

Protonation-induced spectral changes of **1** were also followed by ^1H NMR spectroscopy (Figure 5b and Figure S6) and solution IR spectroscopy (Figure S8a). Upon titration with up to 1 equiv of $HClO_4$, the paramagnetically shifted proton resonances at $\delta = 18$–54 ppm showed significant shifts and broadening, in addition to the appearance of new signals. This process is accompanied by the diminution of strong carbonyl stretching at $\nu = 1606\ cm^{-1}$, which correlates with the build-up of a new feature at $\nu = 1643\ cm^{-1}$ observed by solution IR spectroscopy (Figure S8a). Similar spectral changes were observed when **1** was treated with hard and Lewis acidic Sc^{3+} ion (delivered as $Sc(OTf)_3$ salt) to function as a proton surrogate (Figure S7 and Figure S8b). Back-titration of protonated **1** with Et_3N, however, restored the original spectrum of **1** (Figure 5b and Figure S6). HPLC-MS analysis on the reaction mixture (Figure S9) further established that the reversible changes in both UV/Vis (Figure 5a) and ^1H NMR spectra (Figure 5b and Figure S6) are not associated with protonation-induced demetallation of **1**.

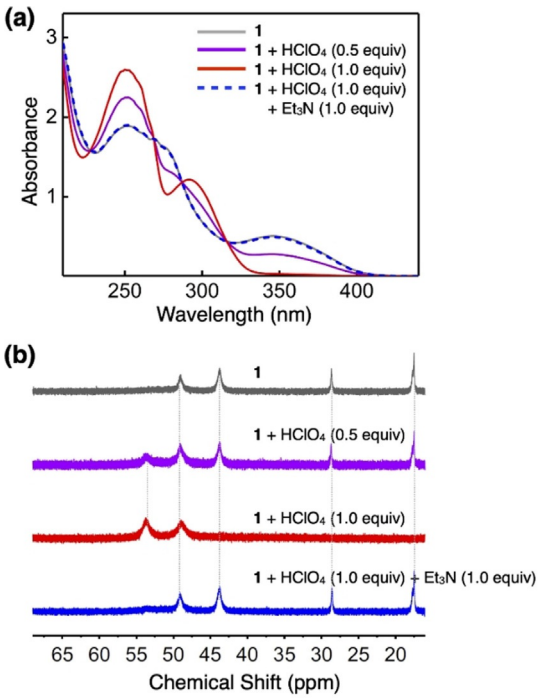

Figure 5. (a) UV/Vis absorption and (b) ^1H NMR spectral changes of **1** in MeCN (concentration = 0.1 mM and 4.0 mM respectively) upon treatment with $HClO_4$ and back-titration with Et_3N at $T = 298$ K.

Low-temperature UV/Vis and EPR studies on the reaction intermediates

With the protonation-gated entry point to the catalytic cycle established, we investigated the nature of the reactive species developing from the initial reaction between the nickel(II) complex and mCPBA (Figure 6). The UV/Vis spectrum of **1** in MeCN showed weak bands at $\lambda_{max} = 540$ nm ($\varepsilon = 30\ cm^{-1}\,M^{-1}$) and $\lambda_{max} = 800$ nm ($\varepsilon = 35\ cm^{-1}\,M^{-1}$). Upon adding 1 equiv of mCPBA to the solution at $-10\,^{\circ}C$, thermally unstable yellow intermediate was formed, which exhibited intense absorption at $\lambda_{max} = 430$ nm ($\varepsilon = 1150\ cm^{-1}\,M^{-1}$) and $\lambda_{max} = 890$ nm ($\varepsilon = 440\ cm^{-1}\,M^{-1}$) and subsequently decayed with $t_{1/2} =$ ca. 200 s (Figure 6a and Figure S10). The X-band EPR spectrum of **1** is featureless (Figure S11), but an axial signal with $g_{\perp} = 2.17$ and $g_{\parallel} = 2.25$ developed upon treatment with 1 equiv of mCPBA

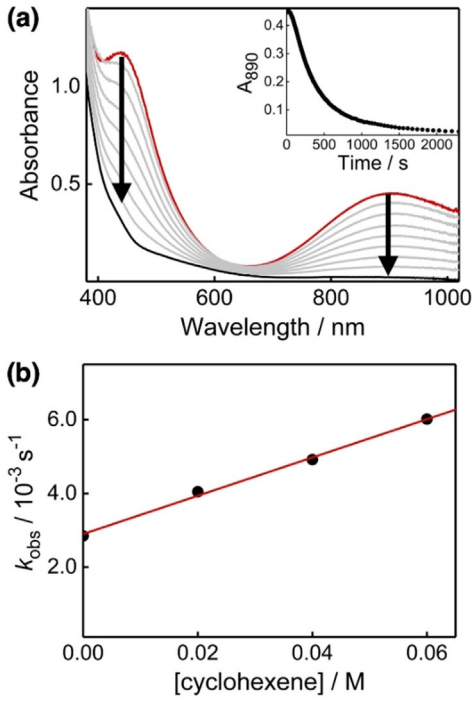

Figure 6. (a) Time-dependent changes in the UV/Vis spectra to follow the thermal decay of the intermediate (red line) generated from the reaction between **1** and mCPBA (1 equiv) in MeCN at $-10\,^{\circ}C$. Inset shows changes in A_{890} (absorbance at $\lambda = 890$ nm) as a function of time. (b) Plot of *pseudo*-first-order rate constants (k_{obs}) vs. the concentration of cyclohexene to determine the second-order rate constant $k_2 = 5.2(\pm 0.2)\times 10^{-2}\,M^{-1}\,s^{-1}$.

(Figure S12), which is characteristic of nickel(III) species with low-spin d^7 ($S = 1/2$) electronic configuration.[12f,j,13a,22]

Unlike the chemistry of high-valent Fe or Mn, studies on nickel-oxo species do not benefit much from the scarce number of well-characterized examples of synthetic origin.[4g,12b] To probe the electronic structure and optical transitions of the yellow intermediate generated from the reaction between **1** and mCPBA, we carried out exploratory DFT and TD-DFT computational studies. As summarized in Table S4, the putative Ni^{III}-oxo species (Figure S13) prefers the $S = 1/2$ spin-state as the ground-state electronic configuration, which is consistent with the experimentally observed EPR spectrum. TD-DFT calculations on this species predicted multiple electronic transitions at around $\lambda = 440$ nm, along with broad and weak band at $\lambda = 800$–1000 nm (Figure S14). While such spectral features are consistent with the low-temperature UV/Vis spectrum shown in Figure 6a, DFT models of high-spin Ni^{III}-oxo ($S = 3/2$) or Ni^{IV}-oxo ($S = 1$) also predicted similar electronic transitions (Figure S14).

To investigate the oxidative reactivity of this yellow intermediate, the reaction between **1** and mCPBA was carried out in the presence of an increasing concentration of cyclohexene substrate. The *pseudo*-first-order rate constants increased proportionally with increasing the concentration of cyclohexene. The second-order rate constant for this bimolecular decay process was determined to be $5.2\times10^{-2}\,M^{-1}\,s^{-1}$ (Figure 6b).[23]

Collectively, our findings suggest that binding of mCPBA is followed by oxidation of nickel(II) to generate reactive intermediate that can be trapped by olefin substrate, although a definitive assignment of the oxidation state and electronic configuration of this intermediate remains currently elusive.

Mechanistic studies of oxidant activation by O–O bond cleavage

What reaction pathways are available for the initial adduct in the catalytic cycle? As a mechanistic probe to address this question, we employed peroxyphenylacetic acid (PPAA) as a terminal oxidant in the epoxidation of olefin by **1**. The chemical structure and relative distribution of the degradation products of PPAA help to understand the mechanism of O–O bond cleavage of the M-OOC(=O)R intermediate.[24] When heterolytic O–O bond cleavage of Ni-OOC(=O)R occurs (Scheme 3, pathway **A**), phenylacetic acid (PAA) is formed. The direct oxidation reaction of substrate by nickel-acylperoxo intermediate affords PAA (pathway **B**). A homolytic O–O bond cleavage of Ni-OOC(=O)R produces a mixture of benzaldehyde (**I**), benzyl alcohol (**II**), and toluene (**III**) through a rapid β-scission of the acyloxy radical intermediate (pathway **C**).

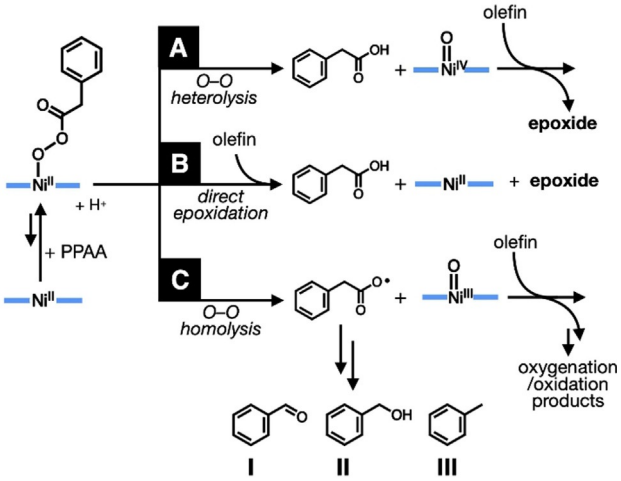

Scheme 3. Reaction pathways of PPAA as mechanistic probe.

We first conducted control experiments on the reaction of **1** with PPAA in the absence of the substrate (Table 3, entry 1). A mixture of the heterolytic cleavage product, phenylacetic acid (60.1%), and the homolytic cleavage products, benzaldehyde (21.3%) and benzyl alcohol (2.9%), were produced. This result indicates that nickel-acylperoxo intermediate underwent both heterolytic cleavage (70%) and homolytic cleavage (30%) to produce putative Ni^{IV}-oxo and Ni^{III}-oxo species, respectively (Scheme 3).

To probe the O–O bond cleavage pattern in the presence of olefin substrate, we employed cyclohexene as a reactive substrate.[24c,d] Even when the concentration of cyclohexene was increased from 0 to 160 mM, the ratios of the heterolysis to homolysis reaction products remained essentially identical (Table 3, entries 1–5). This observation suggests that the Ni-OOC(=O)R intermediate was diverted into heterolytic cleavage (70%) and homolytic cleavage (30%) pathways regardless of the amount of cyclohexene substrate present in the reaction mixture.

To examine the effect of the type of the substrate, we changed the substrate from cyclohexene to 1-octene, which is

Table 3. Analysis of the products derived from PPAA and **1** in the absence or the presence of cyclohexene.[a]

Entry	Cyclohexene (mM)	Heterolysis[b]	Homolysis[b]			Heterolysis/homolysis	Oxidation products[c]		
		PAA	I	II	III	PAA/(I+II+III)	oxide	-one	-ol
1	0	60.1±4.8	21.3±0.5	2.9±2.0	–	2.48	–	–	–
2	20	65.0±0.4	29.4±1.9	0.9±0.1	–	2.14	41.6±0.1[d]	4.8±0.2[d]	3.0±0.1[d]
3	40	63.8±1.6	31.4±1.1	0.8±0.0	–	1.99	26.5±0.3[b]	2.7±0.0[b]	2.0±0.0[b]
4	80	60.2±1.0	29.0±2.6	0.8±0.0	–	2.02	31.3±0.7[b]	3.1±0.5[b]	2.6±0.4[b]
5	160	56.4±2.4	26.3±0.9	0.8±0.0	–	2.09	37.0±0.5[b]	3.6±0.3[b]	3.4±0.3[b]

[a] Reaction conditions: substrate (0–0.16 mmol), **1** (0.0017 mmol), and PPAA (0.04 mmol) in MeCN (1 mL), $T = 25\,^{\circ}C$. [b] Based on PPAA; **I–III** indicate benzaldehyde, benzyl alcohol, and toluene, respectively. [c] Oxide, -one and -ol denote cyclohexene oxide, 2-cyclohexen-1-one, and 2-cyclohexen-1-ol, respectively. [d] Based on the substrate.

more difficult to oxidize. A nearly identical ratio (70:30) of heterolysis to homolysis products was also observed in this case as well (Table S5). These results suggest that **1** effects O–O bond cleavage of the metal-bound acylperoxo species through a combination of heterolysis (70%) and homolysis (30%) pathways, irrespective of the concentration or the type of olefinic substrate present. At the same time, the Ni-OOC(=O)R intermediate species derived from PPAA is not a competent oxidant for olefin epoxidation, or has a short lifetime.

Electronic nature of the reactive intermediate

To gain insights into the electronic nature of the reactive species involved in the olefin epoxidation reaction, we carried out competitive epoxidation reactions of various *para*-substituted styrenes (4-X-$C_6H_4CHCH_2$, X = OMe; Me; H; Cl; CN). The Hammett analysis afforded a ρ value of -0.75 (Figure S15), which indicates the electrophilic nature of the reactive species similar to reported nickel complexes.[12c,g,j,25]

Isotope exchange studies

Isotope exchange experiments help understand the mechanism of catalytic oxygenation reactions. If the high-valent metal-oxo species is sufficiently long lived, its oxygen atom could exchange with exogenously added $H_2{}^{18}O$, so that the solvent-derived oxygen atom ends up in the ^{18}O-labelled oxygenation products.[26] Epoxidation reaction of cyclohexene was thus conducted with **1** and mCPBA in a mixture of distilled MeCN and excess amount (55–220 equiv relative to mCPBA) of $H_2{}^{18}O$ (Table S6). The percentage of ^{18}O incorporated cyclohexene oxide increased from 7.4% to 10.3% with the increasing amount of $H_2{}^{18}O$. This result suggests that a nickel species having solvent-exchangeable oxo ligand is involved as a reactive intermediate in the catalytic cycle.

Mechanism of olefin epoxidation

From the combination of X-ray crystallographic, spectroscopic, kinetic, and mechanistic probe studies, a coherent mechanistic picture emerges, as summarized in Scheme 4. Protonation of the amide carbonyl group of **1** attenuates the electron-donating ability of the ligand, so that mCPBA binds as a ligand to the vacant axial site of $[Ni^{II}(dpap)]^+$ to furnish nickel-acylperoxo intermediate.

The self-regulating nature of this acid-base chemistry is highlighted by a significant decrease in the substrate conversion as well as the epoxidation product yield in the presence of acid ($HClO_4$, Table S7) or base (NH_4OH, Table S8) additives. Exogenously added proton would shift the acid-base equilibrium of mCPBA to suppress its deprotonation, thereby preventing the formation of nickel-acylperoxo intermediate. On the other hand, Brønsted base OH^- functions as a proton scavenger to help convert mCPBA to its conjugate base. Without protonation of the ligand carbonyl group, however, *m*-chloroperbenzoate cannot coordinate to the metal center, and would be diverted away from the catalytic cycle for olefin epoxidation.

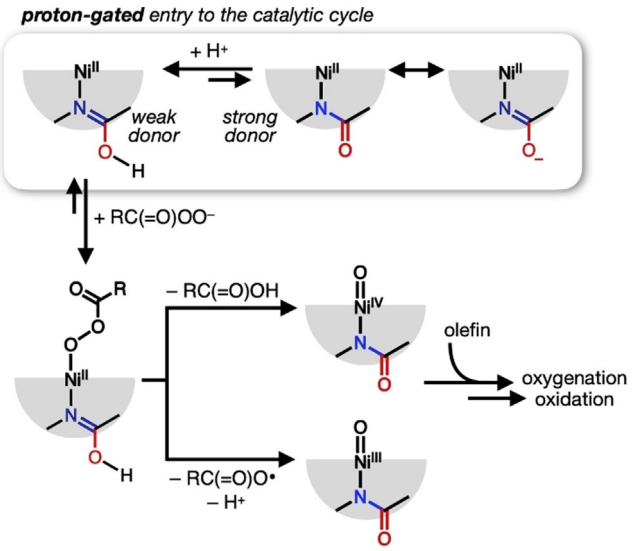

Scheme 4. Mechanism of proton-switched olefin epoxidation via branched reaction pathways.

Based on the mechanistic studies with PPAA, the Ni-OOC(=O)R species partitions into the heterolysis (70%) and homolysis (30%) pathways to afford putative Ni^{IV}-oxo and Ni^{III}-oxo species, respectively, that can exchange with $H_2{}^{18}O$. Presumably, this process is facilitated by the strong σ-donating amido-*N* ligand in the *trans*-position (Scheme 2 and Scheme 4). Understandably, this branching in the reaction coordinate is not affected by the presence of the olefin substrate, as previously been observed.[12j] In contrast, certain nickel-acylperoxo species of porphyrin ligand is competent to effect direct epoxidation of olefins.[12c]

Conclusions

A new monoamidate nickel(II) complex **1** was developed that can efficiently epoxidize various olefins including terminal olefins using mCPBA as a terminal oxidant. To stabilize high-valent nickel-oxo species involved in oxygen-atom transfer, a robust pentadentate chelate H-dpap was built, which functions as a monoanionic ligand by deprotonation of the amide N–H group upon metallation.

We found that protonation of the amide carbonyl group increases the electronic demand of the metal center, so that mCPBA is recruited as a ligand to initiate the catalytic cycle. A combination of spectroscopic, isotope exchange, and product analysis studies using PPAA as a mechanistic probe suggests that O–O bond cleavage of nickel-acylperoxo species generates high-valent nickel-oxo species for subsequent oxygen atom transfer to olefin substrates. For terminal olefins, remarkably high catalytic efficiency and selectivity were observed, which is highly unusual for a nickel-based system.

All chemical reactions can be classified into either substitution or oxidation-reduction.[27] As the smallest and ubiquitous electrophile, the proton nicely couples the non-redox event in the ligand sphere to the redox event at the metal center of **1**. It would be interesting to see if conceptually parallel processes

also occur in the metalloenzymes involved in group-transfer chemistry to shuttle the system between the off-cycle and on-cycle using a proton switch installed at the peptidyl backbone.

Experimental Section

For the full experimental details see the Supporting Information. Deposition number 2015122 contains the supplementary crystallographic data for this paper. These data are provided free of charge by the joint Cambridge Crystallographic Data Centre and Fachinformationszentrum Karlsruhe Access Structures service www.ccdc.cam.ac.uk/structures.

Acknowledgements

This work was supported by the National Research Foundation (NRF) of Korea (2020R1A2C2006381) funded by the Ministry of Science and ICT (MSIT). The work at SNUST and UNIST was supported by NRF (2018R1A2B6001686) and CGRC (2016M3D3A01913243), respectively.

Conflict of interest

The authors declare no conflict of interest.

Keywords: bioinorganic chemistry · enzyme models · epoxidation · ligand design · nickel

[1] a) M. Costas, M. P. Mehn, M. P. Jensen, L. Que, Jr., *Chem. Rev.* **2004**, *104*, 939 – 986; b) A. Decker, E. I. Solomon, *Curr. Opin. Chem. Biol.* **2005**, *9*, 152 – 163; c) P. R. Ortiz de Montellano, *Chem. Rev.* **2010**, *110*, 932 – 948; d) A. J. Jasniewski, L. Que, Jr., *Chem. Rev.* **2018**, *118*, 2554 – 2592; e) H. Park, D. Lee, *Chem. Eur. J.* **2020**, *26*, 5916 – 5926.

[2] a) E. A. Lewis, W. B. Tolman, *Chem. Rev.* **2004**, *104*, 1047 – 1076; b) M. Bordeaux, A. Galarneau, J. Drone, *Angew. Chem. Int. Ed.* **2012**, *51*, 10712 – 10723; *Angew. Chem.* **2012**, *124*, 10870 – 10881; c) S. Sirajuddin, A. C. Rosenzweig, *Biochemistry* **2015**, *54*, 2283 – 2294.

[3] a) V. L. Pecoraro, M. J. Baldwin, A. Gelasco, *Chem. Rev.* **1994**, *94*, 807 – 826; b) R. Manchanda, G. W. Brudvig, R. H. Crabtree, *Coord. Chem. Rev.* **1995**, *144*, 1 – 38; c) S. Sahu, D. P. Goldberg, *J. Am. Chem. Soc.* **2016**, *138*, 11410 – 11428.

[4] a) M. H. Lim, J.-U. Rohde, A. Stubna, M. R. Bukowski, M. Costas, R. Y. N. Ho, E. Münck, W. Nam, L. Que, Jr., *Proc. Natl. Acad. Sci. USA* **2003**, *100*, 3665 – 3670; b) A. S. Borovik, *Chem. Soc. Rev.* **2011**, *40*, 1870 – 1874; c) H. M. Neu, R. A. Baglia, D. P. Goldberg, *Acc. Chem. Res.* **2015**, *48*, 2754 – 2764; d) X. Engelmann, I. Monte-Pérez, K. Ray, *Angew. Chem. Int. Ed.* **2016**, *55*, 7632 – 7649; *Angew. Chem.* **2016**, *128*, 7760 – 7778; e) B. E. R. Snyder, M. L. Bols, R. A. Schoonheydt, B. F. Sels, E. I. Solomon, *Chem. Rev.* **2018**, *118*, 2718 – 2768; f) M. Guo, T. Corona, K. Ray, W. Nam, *ACS Cent. Sci.* **2019**, *5*, 13 – 28; g) V. A. Larson, B. Battistella, K. Ray, N. Lehnert, W. Nam, *Nat. Rev. Chem.* **2020**, *4*, 404 – 419.

[5] a) M. Sono, M. P. Roach, E. D. Coulter, J. H. Dawson, *Chem. Rev.* **1996**, *96*, 2841 – 2888; b) J. N. Rodríguez-López, D. J. Lowe, J. Hernández-Ruiz, A. N. P. Hiner, F. García-Cánovas, R. N. F. Thorneley, *J. Am. Chem. Soc.* **2001**, *123*, 11838 – 11847; c) J. S. de Ropp, S. Sham, A. Asokan, S. L. Newmyer, P. R. Ortiz de Montellano, G. N. La Mar, *J. Am. Chem. Soc.* **2002**, *124*, 11029 – 11037.

[6] C. Panda, A. Sarkar, S. Sen Gupta, *Coord. Chem. Rev.* **2020**, *417*, 213314.

[7] a) M. Kobayashi, S. Shimizu, *Curr. Opin. Chem. Biol.* **2000**, *4*, 95 – 102; b) A. Miyanaga, S. Fushinobu, K. Ito, T. Wakagi, *Biochem. Biophys. Res. Commun.* **2001**, *288*, 1169 – 1174.

[8] a) A. Miyanaga, S. Fushinobu, K. Ito, H. Shoun, T. Wakagi, *Eur. J. Biochem.* **2004**, *271*, 429 – 438; b) T. Yano, H. Arii, S. Yamaguchi, Y. Funahashi, K. Jitsukawa, T. Ozawa, H. Masuda, *Eur. J. Inorg. Chem.* **2006**, 3753 – 3761; c) M. Prejanò, T. Marino, C. Rizzuto, J. C. Madrid, N. Russo, M. Toscano, *Inorg. Chem.* **2017**, *56*, 13390 – 13400.

[9] a) D. P. Barondeau, C. J. Kassmann, C. K. Bruns, J. A. Tainer, E. D. Getzoff, *Biochemistry* **2004**, *43*, 8038 – 8047; b) J. Wuerges, J.-W. Lee, Y.-I. Yim, H.-S. Yim, S.-O. Kang, K. D. Carugo, *Proc. Natl. Acad. Sci. USA* **2004**, *101*, 8569 – 8574.

[10] M. J. Maroney, S. Ciurli, *Chem. Rev.* **2014**, *114*, 4206 – 4228.

[11] a) J. Shearer, *Acc. Chem. Res.* **2014**, *47*, 2332 – 2341; b) J. O. Campeciño, L. W. Dudycz, D. Tumelty, V. Berg, D. E. Cabelli, M. J. Maroney, *J. Am. Chem. Soc.* **2015**, *137*, 9044 – 9052.

[12] a) M. Sankaralingam, M. Balamurugan, M. Palaniandavar, P. Vadivelu, C. H. Suresh, *Chem. Eur. J.* **2014**, *20*, 11346 – 11361; b) T. Corona, A. Company, *Chem. Eur. J.* **2016**, *22*, 13422 – 13429; c) H. M. Ahn, J. M. Bae, M. J. Kim, K. H. Bok, H. Y. Jeong, S. J. Lee, C. Kim, *Chem. Eur. J.* **2017**, *23*, 11969 – 11976; d) S. K. Padamati, D. Angelone, A. Draksharapu, G. Primi, D. J. Martin, M. Tromp, M. Swart, W. R. Browne, *J. Am. Chem. Soc.* **2017**, *139*, 8718 – 8724; e) M. Sankaralingam, M. Balamurugan, M. Palaniandavar, *Coord. Chem. Rev.* **2020**, *403*, 213085; f) F. F. Pfaff, F. Heims, S. Kundu, S. Mebs, K. Ray, *Chem. Commun.* **2012**, *48*, 3730 – 3732; g) T. Corona, F. F. Pfaff, F. Acuña-Parés, A. Draksharapu, C. J. Whiteoak, V. Martin-Diaconescu, J. Lloret-Fillol, W. R. Browne, K. Ray, A. Company, *Chem. Eur. J.* **2015**, *21*, 15029 – 15038; h) T. Corona, A. Draksharapu, S. K. Padamati, I. Gamba, V. Martin-Diaconescu, F. Acuña-Parés, W. R. Browne, A. Company, *J. Am. Chem. Soc.* **2016**, *138*, 12987 – 12996; i) P. Pirovano, E. R. Farquhar, M. Swart, A. R. McDonald, *J. Am. Chem. Soc.* **2016**, *138*, 14362 – 14370; j) K. H. Bok, M. M. Lee, G. R. You, H. M. Ahn, K. Y. Ryu, S.-J. Kim, Y. Kim, C. Kim, *Chem. Eur. J.* **2017**, *23*, 3117 – 3125; k) J. Singh, G. Hundal, R. Gupta, *Eur. J. Inorg. Chem.* **2008**, 2052 – 2063.

[13] a) A. R. Jeong, J. W. Shin, J. H. Jeong, K. H. Bok, C. Kim, D. Jeong, J. Cho, S. Hayami, K. S. Min, *Chem. Eur. J.* **2017**, *23*, 3023 – 3033; b) D. Chatterjee, S. Mukherjee, A. Mitra, *J. Mol. Catal. A* **2000**, *154*, 5 – 8; c) M. T. Rispens, O. J. Gelling, A. H. M. de Vries, A. Meetsma, F. van Bolhuis, B. L. Feringa, *Tetrahedron* **1996**, *52*, 3521 – 3546.

[14] a) J. P. Collman, Z. Wang, A. Straumanis, M. Quelquejeu, *J. Am. Chem. Soc.* **1999**, *121*, 460 – 461; b) H. Tian, X. She, J. Xu, Y. Shi, *Org. Lett.* **2001**, *3*, 1929 – 1931; c) M. C. White, A. G. Doyle, E. N. Jacobsen, *J. Am. Chem. Soc.* **2001**, *123*, 7194 – 7195; d) A. Murphy, T. D. P. Stack, *J. Mol. Catal. A: Chem.* **2006**, *251*, 78 – 88; e) I. Garcia-Bosch, X. Ribas, M. Costas, *Adv. Synth. Catal.* **2009**, *351*, 348 – 352.

[15] H. Park, H. M. Ahn, H. Y. Jeong, C. Kim, D. Lee, *Chem. Eur. J.* **2018**, *24*, 8632 – 8638.

[16] a) S. Hong, Y.-M. Lee, M. Sankaralingam, A. K. Vardhaman, Y. J. Park, K.-B. Cho, T. Ogura, R. Sarangi, S. Fukuzumi, W. Nam, *J. Am. Chem. Soc.* **2016**, *138*, 8523 – 8532; b) D. B. Rice, E. N. Grotemeyer, A. M. Donovan, T. A. Jackson, *Inorg. Chem.* **2020**, *59*, 2689 – 2700; c) S.-S. Xue, X.-X. Li, Y.-M. Lee, M. S. Seo, Y. Kim, S. Yanagisawa, M. Kubo, Y.-K. Jeon, W.-S. Kim, R. Sarangi, S. H. Kim, S. Fukuzumi, W. Nam, *J. Am. Chem. Soc.* **2020**, *142*, 15305 – 15319.

[17] C. Incarvito, A. L. Rheingold, A. L. Gavrilova, C. J. Qin, B. Bosnich, *Inorg. Chem.* **2001**, *40*, 4101 – 4108.

[18] a) D. M. L. Goodgame, D. J. Williams, R. E. P. Winpenny, *Polyhedron* **1989**, *8*, 1913 – 1921; b) J.-P. Costes, F. Dahan, B. Donnadieu, M.-J. Rodriguez Douton, M.-I. Fernandez Garcia, A. Bousseksou, J.-P. Tuchagues, *Inorg. Chem.* **2004**, *43*, 2736 – 2744.

[19] a) C. Bousquet, D. G. Gilheany, *Tetrahedron Lett.* **1995**, *36*, 7739 – 7742; b) R. V. Ottenbacher, D. G. Samsonenko, E. P. Talsi, K. P. Bryliakov, *ACS Catal.* **2016**, *6*, 979 – 988.

[20] a) W. Adam, C. Mock-Knoblauch, C. R. Saha-Möller, M. Herderich, *J. Am. Chem. Soc.* **2000**, *122*, 9685 – 9691; b) C. Linde, M. F. Anderlund, B. Åkermark, *Tetrahedron Lett.* **2005**, *46*, 5597 – 5600.

[21] a) S. H. van Rijt, A. J. Hebden, T. Amaresekera, R. J. Deeth, G. J. Clarkson, S. Parsons, P. C. McGowan, P. J. Sadler, *J. Med. Chem.* **2009**, *52*, 7753 – 7764; b) R. M. Lord, S. J. Allison, K. Rafferty, L. Ghandhi, C. M. Pask, P. C. McGowan, *Dalton Trans.* **2016**, *45*, 13196 – 13203.

[22] R. I. Haines, A. McAuley, *Coord. Chem. Rev.* **1981**, *39*, 77 – 119.

[23] While the involvement of multiple reaction pathways (Schemes 3 and 4) makes the interpretation of the rate constant k_2 less than straightforward, the linear relationship between k_{obs} and [olefin] unambiguously establishes the bimolecular nature of the reaction mechanism.

[24] a) T. G. Traylor, S. Tsuchiya, Y. S. Byun, C. Kim, *J. Am. Chem. Soc.* **1993**, *115*, 2775 – 2781; b) W. Nam, H. J. Choi, H. J. Han, S. H. Cho, H. J. Lee, S.-Y. Han, *Chem. Commun.* **1999**, 387 – 388; c) N. Suzuki, T. Higuchi, T. Nagano, *J. Am. Chem. Soc.* **2002**, *124*, 9622 – 9628; d) M. Y. Hyun, Y. D. Jo, J. H. Lee, H. G. Lee, H. M. Park, I. H. Hwang, K. B. Kim, S. J. Lee, C. Kim, *Chem. Eur. J.* **2013**, *19*, 1810 – 1818.
[25] J. Nakazawa, S. Terada, M. Yamada, S. Hikichi, *J. Am. Chem. Soc.* **2013**, *135*, 6010 – 6013.
[26] a) K. A. Lee, W. Nam, *J. Am. Chem. Soc.* **1997**, *119*, 1916 – 1922; b) K. Nehru, S. J. Kim, I. Y. Kim, M. S. Seo, Y. Kim, S.-J. Kim, J. Kim, W. Nam, *Chem. Commun.* **2007**, 4623 – 4625.
[27] H. Taube, *Science* **1984**, *226*, 1028 – 1036.

Manuscript received: December 2, 2020
Accepted manuscript online: January 11, 2021
Version of record online: February 5, 2021